ChemPlusChem

Research Article
doi.org/10.1002/cplu.202300484

Chemistry Europe
European Chemical Societies Publishing

www.chempluschem.org

Special Collection

Production of Highly Efficient Activated Carbons for Wastewater Treatment from Post-Consumer PET Plastic Bottle Waste

Olajumoke Alabi-Babalola,[a, b] Elizabeth Aransiola,[b] Edidiong Asuquo,[a] Arthur Garforth,[a] and Carmine D'Agostino*[a, c]

Chemical activated carbons (PET-H_2SO_4 and PET-KOH) were prepared from post-consumer polyethylene terephthalate (PET) wastes using pyrolysis under moderate reaction temperatures by changing pyrolysis time and chemical activating agents. The produced carbons were characterized and tested in adsorption reactions of manganese, chromium, and cobalt ions in aqueous solutions. Results showed a high percentage removal of these inorganic ions from water: 98% for Mn^{2+}, 87% for Cr^{3+}, and 88% for Co^{2+}. Freundlich isotherms gave a better fit to the experimental data obtained with good correlation coefficient values in the range of 0.99-1 compared to other isotherms. The pseudo-second order kinetic model best described the chemical adsorption process as an exchange of electrons between the carbon and inorganic ions in solutions. The diffusion models showed that the process is controlled by a multi-kinetic stage adsorption process. In summary, this work demonstrates that the production of activated carbon from PET waste bottles is a potential alternative to commercial activated carbon and can be considered a sustainable waste management technology for removing these non-biodegradable plastic wastes from the environment.

Introduction

Plastics have been widely used and are ubiquitous in our daily lives. They have been promoted worldwide due to their favourable physico-chemical properties such as light weight, low cost, and chemical stability. The global annual production of plastics has risen considerably over the past few decades with an annual increase of about 5% per annum.[1] The increased demand of these polymers has led to rapid accumulation of wastes, thus, creating serious environmental pollution problems and posing a threat to human health. Polymer wastes are mainly being recycled *via* three (3) methods: mechanical, energy and chemical.[2]

[a] O. Alabi-Babalola, Dr. E. Asuquo, Dr. A. Garforth, Dr. C. D'Agostino
Department of Chemical Engineering
The University of Manchester
Oxford Road
Manchester M13 9PL (UK)
E-mail: carmine.dagostino@manchester.ac.uk

[b] O. Alabi-Babalola, Dr. E. Aransiola
Department of Chemical Engineering
Obafemi Awolowo University
Ile-Ife (Nigeria)

[c] Dr. C. D'Agostino
Dipartimento di Ingegneria Civile, Chimica, Ambientale e dei Materiali (DICAM)
Alma Mater Studiorum – Università di Bologna
Via Terracini, 28
40131 Bologna (Italy)

Special Collection Part of a Special Collection on Green Chemistry

In mechanical recycling, the macromolecular structure remains unchanged and the material is transformed into new polymer products. In this case, the polymer waste is grinded or remelted and then mixed with virgin resin or other additives such as crosslinking agents, and surfactants.[3] However, this is a very challenging and difficult approach[2] as there are usually material defects in the reformed polymer compared to the original item. Energy recycling involves the use of incineration technologies where thermal/heat energy is produced.[4] Chemical recycling involves the conversion of these wastes into relatively new materials, which are subsequently used as industrial feedstocks.[5] Different products can be produced depending on the technologies involved.

The different protocols that can be employed in chemical recycling of polymer wastes include pyrolysis, catalytic cracking, thermal cracking, and hydrocracking, yielding products, such as gaseous fuels, liquid fuels, and carbon.[6] The transformation of plastic wastes into useful products to remediate environmental problems has been reported by several authors. This include the valorisation of waste plastics for carbon and hydrogen production,[7,8] capture, storage, and utilization.[9–11] Several authors have also reported the treatment of oil spills[12,13] *via* the upcycling of waste plastics such as polypropylene masks,[14] high density polyethylene (HDPE) wastes,[15] polystyrene wastes,[16] polyethylene and polypropylene waste powder and sheets.[17] In recent studies, waste plastics have been subjected to post-synthetic chemical modification to form functional catalysts and polymers[18–20] as well as development of fluorescent carbon for sensing toxic chemicals.[21,22]

Activated carbon (AC) produced from pyrolysis of post-consumer wastes has evolved and is targeted at achieving a friendly technology to produce relatively inexpensive carbon

with good adsorption properties as a substitute for commercial activated carbon. Different precursors have been utilized in the production of activated carbon, mostly agricultural by-products, wood, synthetic resins, industrial wastes.[23–26] Factors usually considered are cost, availability/renewability of the material, and the carbon content of the precursor. The production of activated carbons from plastic waste is a sustainable technology targeted at solving environmental pollution problems associated with the increasing demand of these polymers.

Although some polyethylene terephthalate (PET) wastes are being tried to be recycled mechanically, the success of the recycling process largely depends on the efficient sorting of the bottles (waste logistics), and degree of purification/decontamination during processing, which is not fully guaranteed. Moreover, due to its high decomposition temperature (about 280 °C), common organic impurities such as PVC, polyolefins, polyvinyl acetate, colouring agents, melt adhesive, sugar and protein residues, and chemical wood-pulp are transformed into coloured degradation products during the recycling process. The required high decomposition temperature results in excess reactive degradation products, and subsequently, increases the frequency of defects present within the polymer chain. Moreover, the presence of visible and microscopic particles (impurities) may also increase the amounts of defects within the polymer.

Several examples have been reported for the upcycling of PET wastes into useful products. These include their conversion into lithium-anode batteries in the form of metal-organic framework,[27] porous carbons for CF_4 capture,[28] polymer electrolytes,[29] redox-active nanoparticles for energy storage applications,[30,31] magnetic microparticles for adsorption,[32] hydrogel adsorbents *via* crosslinking and aminolysis.[33]

In the work reported here, we investigate conversion of PET bottles into activated carbon using pyrolysis, under controlled reaction temperature and time. This conversion is followed by the chemical activation of the produced carbon using acid and base activating agents. The effect of pyrolysis temperature, pyrolysis time, and concentration of activating agents are investigated by adsorption and kinetic studies of the carbons in the removal of inorganic ions from water. The performance indicators are the iodine values, carbon yield, and adsorption capacities.

Results and discussion

Thermal degradation of PET

The thermal decomposition of PET occurs by a random chain scission of the ester linkage or through chain ends and is initiated by the breaking of an alkyl-oxygen bond.[34] The thermal degradation occurs through the formation of different end groups such as vinyl ester, cyclic or open chain oligomers with olefinic or carboxyl end groups giving rise to gaseous products such as: carbon monoxide, carbon dioxide, water, acetaldehyde, and compounds with acid and anhydride end groups. This results in a decrease in the molecular weight of the polymer. The monomer structure is shown in Figure 1.

The thermal degradation plots for PET wastes at different heating rates of 5, 10, and 20 °C/min are shown in Figure 2. The results obtained reveal that the decomposition temperature of the polymer wastes increases with increasing heating rates. Prior to decomposition, a relatively constant-weight process is observed up to about 250 °C (indicating a low amount of moisture), followed by a continuous decrease in weight up to temperatures of approximately 480 °C. During this process, there is an evolution of volatile organic hydrocarbons associated with the nature of the precursors, leading to a significant weight loss of approximately 74 %. At different heating rates of 5, 10, and 20 °C/min, the decomposition occurs at 361 °C, 372 °C, and 395 °C, and reaches a maximum at 419, 432, and 443 °C, respectively. As the degradation progresses, a final thermal zone of constant weight is obtained, which indicates the formation of carbon.

The solid residue left behind during the thermal decomposition of these polymers is known as the carbonized char and the amount obtained expressed in percentage is referred to as the activated carbon yield. AC produced from acid-activated PET bottles is designated as PET-H_2SO_4 while the base-activated PET bottle wastes as PET-KOH. The chemical activating agents introduced on the carbon surfaces act as both dehydrating and oxidizing agents, which helps in the formation of oxygen-containing functional groups, such as carbonyl groups. Tables 1 and 2 show the effect of pyrolysis temperature, time and concentration of activating agents on the physico-chemical properties of the activated carbon.

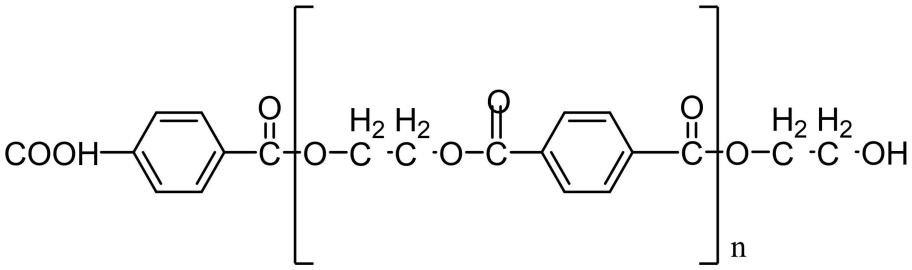

Figure 1. Polyethylene terephthalate (PET).

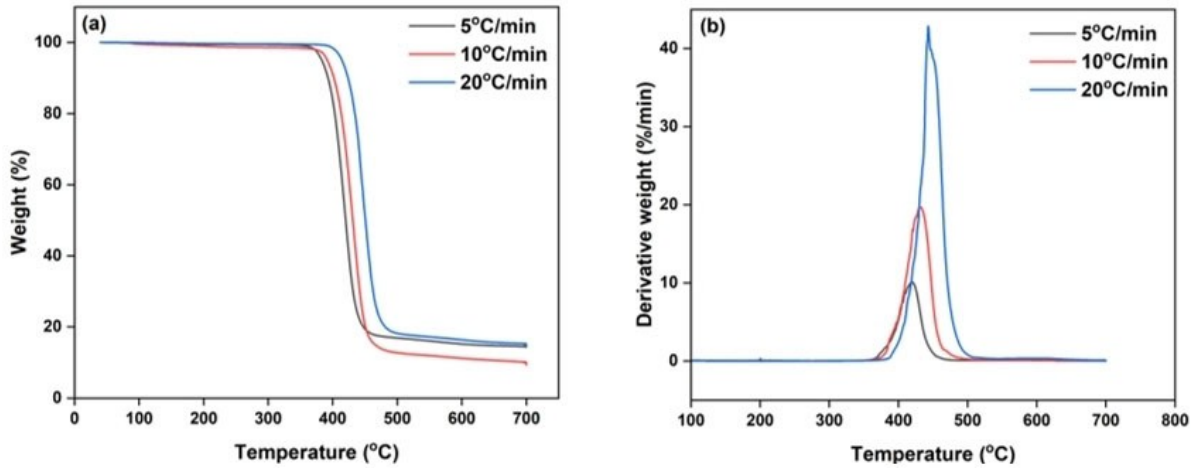

Figure 2. Thermograms of PET waste (a) TGA (b) derivative-TGA curve.

Table 1. Effect of reaction conditions on physico-chemical properties of PET-H_2SO_4.

Runs	Reaction conditions				Physico-chemical properties						
	Temp. (°C)	Time (min)	Conc. (mol/L)	Activated yield (%)	Moisture content (%)	Bulk density (g/cm^3)	Ash content (%)	Iodine value (mg/g)	% $(MnO_4)^-$ removal	% $(Cr_2O_7)^{2-}$ removal	% Co^{2+} removal
1	400	60	0.5	31	5	0.472	26	2175	96	83	85
2	400	45	0.5	34	6	0.491	21	1879	95	82	85
3	400	60	1.25	27	10	0.431	25	2075	96	85	86
4	400	45	1.25	35	9	0.471	19	1690	94	83	83
5	400	45	2.0	37	8	0.483	20	1302	94	83	84
6	400	60	2.0	33	7	0.491	23	1650	95	84	85
7	450	60	1.25	28	5	0.442	25	2099	97	87	88
8	450	45	1.25	34	7	0.482	20	1613	94	80	80
9	500	45	0.5	29	5	0.483	23	2042	96	84	86
10	500	60	0.5	26	5	0.451	30	2213	97	86	85
11	500	60	2.0	28	5	0.475	20	1692	96	84	85
12	500	45	2.0	31	8	0.481	21	1513	96	84	86

Physicochemical characterization

The physico-chemical characteristics of the modified carbons are shown in Tables 1 and 2. Figure 3 shows the effect of pyrolysis temperature and time on the carbon yield. It is seen that a maximum carbonized yield of 37% occurs at a pyrolysis temperature of 400 °C, time of 45 mins, and concentration of 2.0 M for the polymer waste. Conversely, the lowest carbon yield was obtained at reaction conditions of 500 °C and 60 mins. This low carbon yield implies that as the pyrolysis temperature increases and time progresses, the polymer melt decomposes into more liquid and gaseous fuel products *via* different organic reactions, thus reducing the amount of coke residue product.

The amount of moisture content is similar for all produced carbons and is in the range of 4–8% while the bulk density also have similar values with no significant difference. The iodine value is a fundamental property that evaluates the adsorption capacity of the carbons as well as their surface area. It helps to evaluate the activity levels of the AC (a higher iodine value indicates higher degree of activation, and vice-versa).[35] Both acid- and base-activated carbons have similar iodine numbers, thus, suggesting a similar degree of activation.

As reaction time increased the iodine number also increased (Figure 4). Both acid-activated (PET-H_2SO_4) and base-activated carbons (PET-KOH) have relatively similar iodine values within the experimental uncertainty, thus, suggesting that the use of both H_2SO_4 and KOH as chemical activating agents helps in the development of the porous carbon structures.

The activated carbons produced have high affinity for inorganic ions (Figure 5 and 6). The adsorption of manganese ions from the aqueous solutions is in the range of 90–98% and this implies that there is a high affinity of the carbons towards manganese ions, in which case the deep purple colour of $[MnO_4]^-$ changes to a colourless Mn^{2+}. Our results show

Table 2. Effect of reaction conditions on physico-chemical properties of PET-KOH.

Runs	Reaction conditions			Physico-chemical properties							
	Temp. (°C)	Time (min)	Conc. (mol/L)	Activated yield (%)	Moisture content (%)	Bulk density (g/cm^3)	Ash content (%)	Iodine value (mg/g)	% $(MnO_4)^-$ removal	% $(Cr_2O_7)^{2-}$ removal	% Co^{2+} removal
1	400	60	0.5	30	5	0.461	22	2154	93	70	81
2	400	45	0.5	34	5	0.482	16	1862	92	70	82
3	400	60	1.25	28	9	0.425	25	1998	94	72	83
4	400	45	1.25	36	10	0..465	19	1586	92	70	80
5	400	45	2.0	37	8	0.476	16	1276	92	70	82
6	400	60	2.0	34	7	0.472	20	1600	95	72	80
7	450	60	1.25	29	4	0.419	21	2076	96	74	84
8	450	45	1.25	35	7	0.471	20	1614	91	69	79
9	500	45	0.5	29	5	0.475	18	1979	94	71	83
10	500	60	0.5	27	5	0.452	28	2198	95	73	83
11	500	60	2.0	29	5	0.462	20	1601	95	73	83
12	500	45	2.0	32	10	0.453	21	1464	93	71	87

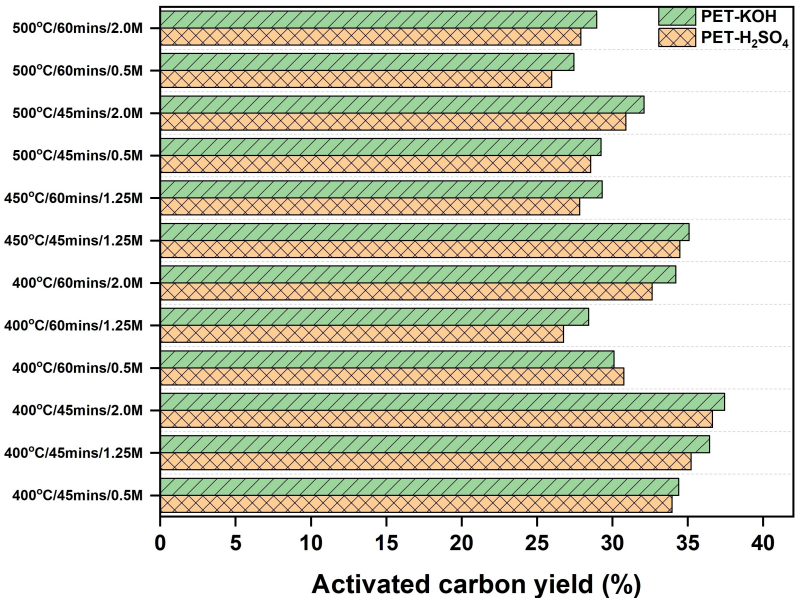

Figure 3. Effect of process conditions on activated carbon yield.

adsorption capacities which are higher[36,37] or in line[38] with those reported for uptake of manganese ions using carbon-based adsorbents. This is a strong indication that our precursor (PET wastes) are valuable starting materials to produce activated carbon. The removal capacity of the carbon for $[Cr_2O_7]^{2-}$ is relatively low compared to those of manganese ions and is in the range of 69–87 %, while that of cobalt ions falls within 70–88 %. These results are similar to those reported in the literature.[39] The ionic equations are shown in Equations 1 and 2.

$$MnO_4^- + 8H^+ + 5e^- \rightarrow Mn^{2+} + 4H_2O \quad (1)$$

$$Cr_2O_7^{2-} + 14H^+ + 6e^- \rightarrow 2Cr^{3+} + 7H_2O \quad (2)$$

It is interesting to note that carbons produced at 450 °C, 60 mins, and 1.25 M gave the best removal capacity. Hence, they were further characterized and the acid-activated carbon was used for subsequent isotherm and kinetic studies.

Characterization results

FTIR analysis shown in Figure 7a shows the presence of the functional groups similar to those of activated carbons. [23, 40, 41] The peaks between 1500–1671 cm^{-1} correspond to C=O stretching vibrations, while the peak at 2359 cm^{-1} corresponds

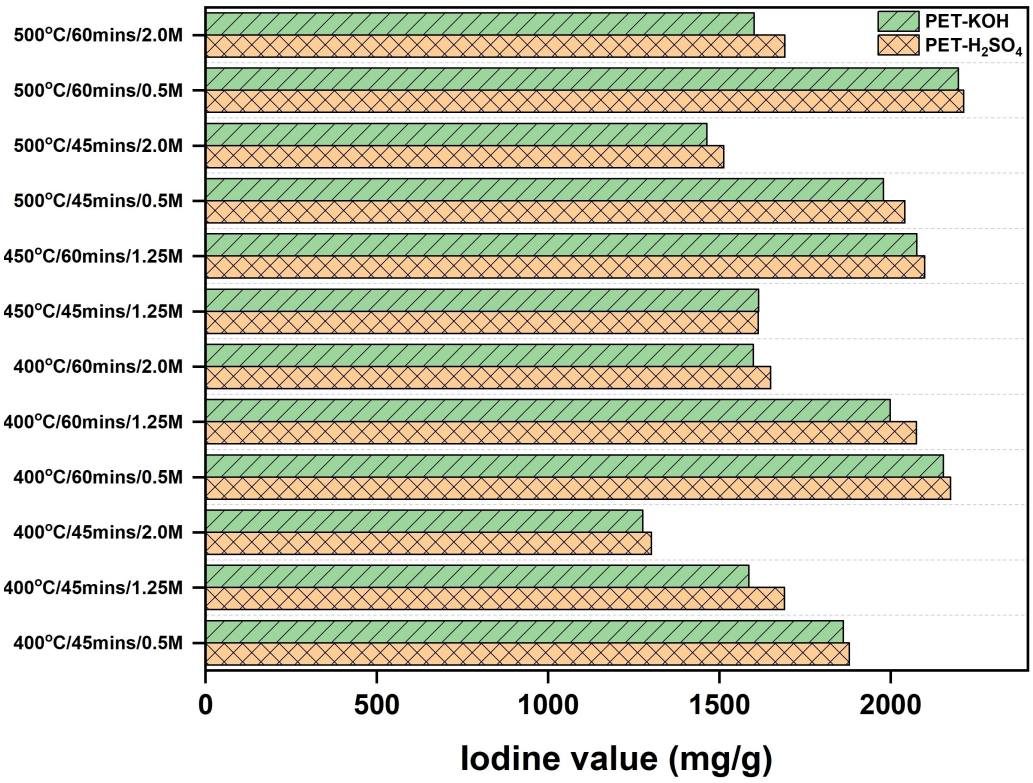

Figure 4. Effect of process conditions on iodine values of activated carbons produced from PET.

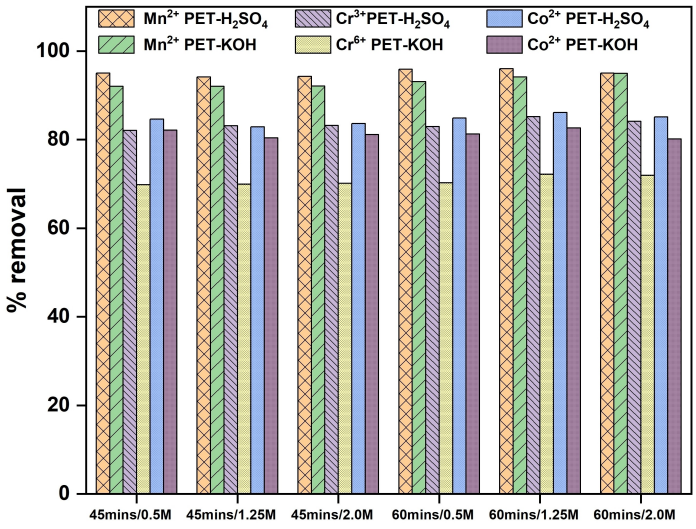

Figure 5. Adsorption performance of acid- and base-activated carbons produced at 400 °C.

to strong O=C=O stretching vibration. This result is a good indication that the surface of the activated carbons is rich in oxygen species arising from chemical activation. X-ray diffraction analysis as illustrated in Figure 7b shows a good dispersion of both H_2SO_4 and KOH on the surface of the carbons rather than a low concentration of these impregnated chemicals as there are no specific peaks associated with the acid or base presence on the carbon surface. The BET surface area of PET-H_2SO_4 and KOH were found to be 57.37 m^2/g and 51.98 m^2/g, respectively.

Adsorption analysis

The activated carbon produced at 450 °C, 60 mins, 1.25 M PET-H_2SO_4 was found to have the highest removal capacity from preliminary studies and was subsequently used for the

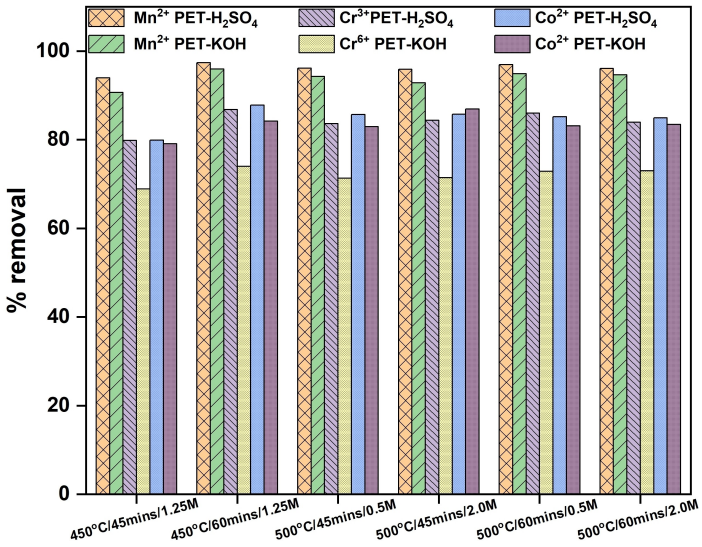

Figure 6. Adsorption performance of acid- and base-activated carbons produced at 450 °C and 500 °C.

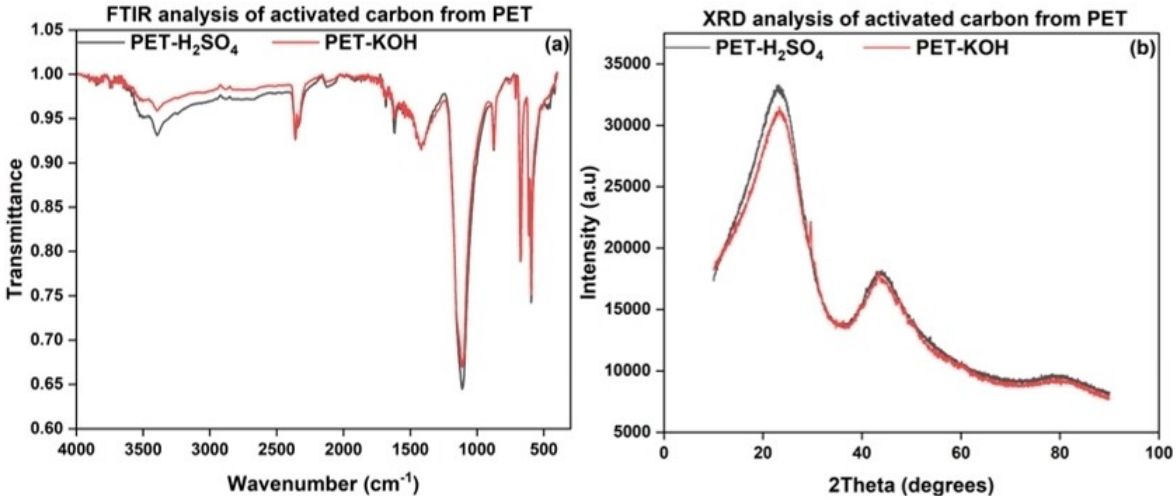

Figure 7. Characterization of chemical activated carbons (a) FTIR (b) XRD.

adsorption and kinetic studies. The equilibrium data obtained were analyzed using the linearized forms of the Langmuir, Freundlich, Temkim, and Dubinin-Radushkevich (D-R) adsorption isotherms models expressed in Equations 3, 4, 5, and 6 respectively:

$$\frac{C_e}{q_e} = \frac{1}{K_L b Q_0} + \frac{C_e}{Q_0} \tag{3}$$

$$\log q_e = log K_f + \frac{1}{n} log C_e \tag{4}$$

$$q_e = \frac{RT}{b_T} ln A_T + \left(\frac{RT}{b_T}\right) \ln C_e \tag{5}$$

$$\ln(q_e) = \ln(q_s) - K_{ad}\varepsilon^2 \tag{6}$$

where $C_e$is the equilibrium concentration (mg/L), C_o is the initial concentration of the adsorbate (mg/L), q_e is the amount of adsorbate present in the adsorbent at equilibrium (mg/g), K_L represents the Langmuir constant (dm^3/mg), Q_0 denotes the maximum monolayer coverage (mg/g), K_f the Freundlich isotherm constant (mg/g)(dm^3/g)^n, n represents the intensity of adsorption, R is the Universal gas constant (J/mol K), T temperature (K), A_T the Temkin isotherm equilibrium binding constant (L/g), b_T is the Temkin isotherm constant, q_s the theroretical isotherm saturation capacity (mg/g), K_{ad} denotes the D-R isotherm constant (mol^2/kJ^2), and ε is the D-R isotherm constant.

The experimental data were fitted to the different isotherm models as shown in Figures 8(a)–(d) and the parameters were evaluated as shown in Table 3 in order to explain the behaviour of the systems under investigation. The coefficient of determination (R^2) was obtained using the expression (Equation 7):

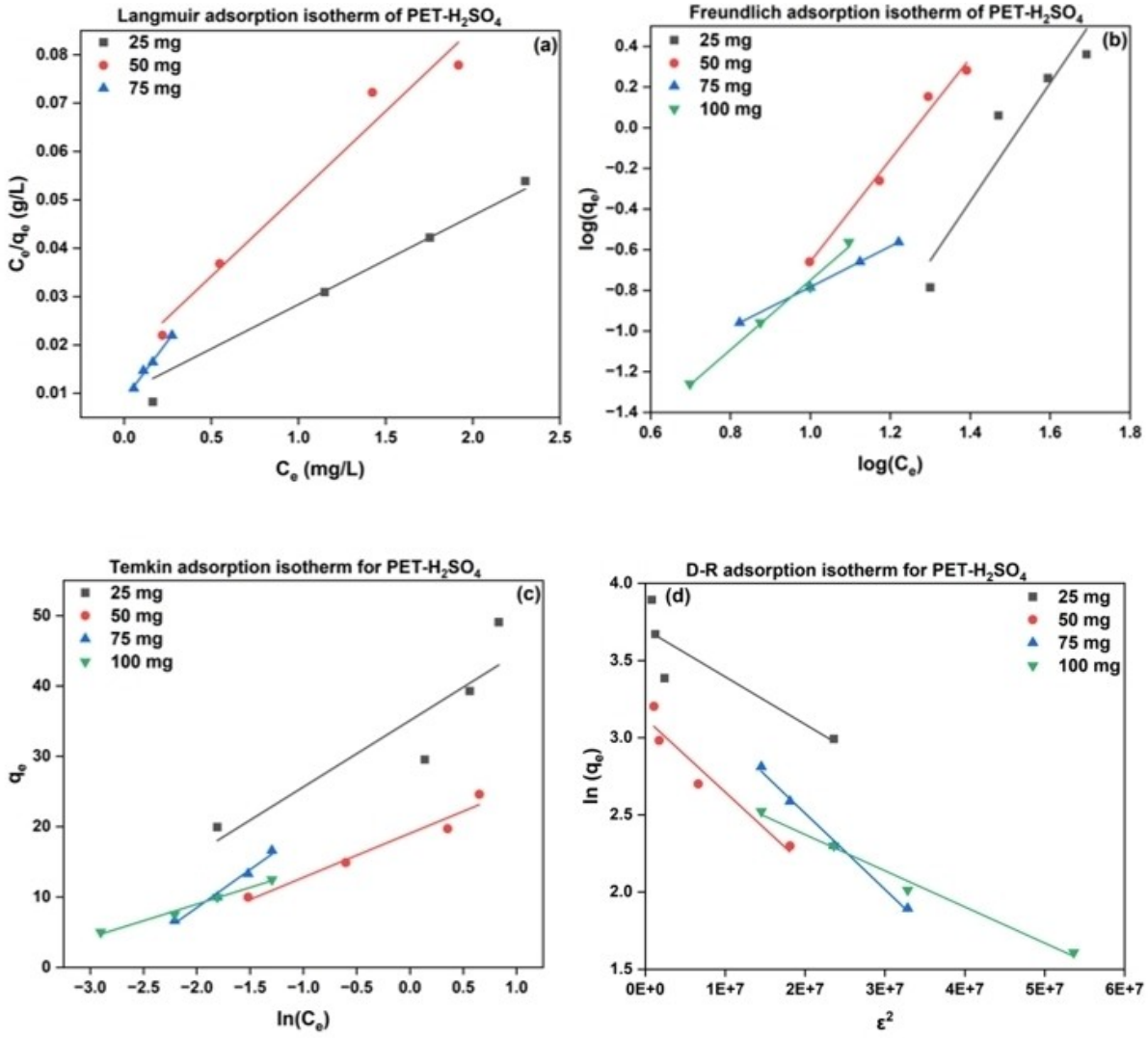

Figure 8. Adsorption isotherm studies of PET-H_2SO_4 (a) Langmuir (b) Freundlich (c) Temkin

Table 3. Adsorption parameter constants for PET-H_2SO_4 at 450 °C, 60 mins, 1.25 M.

Adsorbent dosage (mg)		Adsorption isotherms					
		Langmuir			Freundlich		
	Q_0 (mg/g)	K_L (L/mg)	R^2	R_L	K_f (mg/g).(L/g)^n	n	R^2
25	47.081	4.008	0.993	0.005	3.654E-05	0.343	0.899
50	29.274	1.993	0.968	0.010	6.936E-04	0.400	0.985
75	20.589	5.583	0.993	0.004	1.663E-02	1.004	1.000
100	Fitting not reliable				3.481E-03	0.585	0.991
		Temkin			Dubnin-Radushkevich		
		A_T (L/g)	b_T	R^2	q_s (mg/g)	K_{ad} (mol^2/kJ^2)	R^2
25		40.929	262.062	0.811	40.506	40.506	0.767
50		20.864	395.451	0.959	22.749	22.749	0.926
75		16.194	229.440	0.983	33.110	33.110	0.995
100		49.524	524.973	0.988	17.162	17.162	0.990

$$R^2 = \frac{\left(q_{e,meas} - \overline{q_{e,calc}}\right)^2}{\sum \left(q_{e,meas} - \overline{q_{e,calc}}\right)^2 + \left(q_{e,meas} - q_{e,calc}\right)^2} \quad (7)$$

Langmuir isotherms produced good R-squared values between 0.97 and 0.99. However, the isotherm study using 100 mg of carbon gave poor R-squared value, hence, it was ignored. A separation factor R_L defined by Weber and Chakkravorti[42] expressed in Equation 8, is often used to determine the nature of the adsorption process.

$$R_L = \frac{1}{K_L C_o} \quad (8)$$

Adsorption is linear if $R_L = 1$, favourable if $0 < R_L < 1$, unfavourable if $R_L > 1$, and irreversible if $R_L = 0$. R_L values obtained from this work indicates a favourable adsorption process.

The Freundlich parameter n is an indication of the extent of heterogeneity, or otherwise, of the adsorption process. Values of $\frac{1}{n} > 1$ indicate a cooperative adsorption and when $\frac{1}{n} < 1$ imply a chemisorption process.[43] As the slope of the Freundlich isotherm gets closer to zero, the more heterogeneous the adsorption process becomes. The Freundlich slope values $\frac{1}{n}$ obtained in our work showed values in the range (1–2.9); thus indicating a favourable, less heterogeneous adsorption process.[37] The coefficient of determination values are in the range of 0.9 to 1.

The Temkin isotherm explains the adsorbent-adsorbate interactions and assumes that the heat of adsorption of the adsorbate layer molecules will decrease linearly and not logarithmically. The Temkin isotherm plot gave a good fit at higher adsorbent dosage of 75 mg and 100 mg with good R-squared values of 0.98 and 0.99, respectively. Conversely, the D-R plot, which expresses the diffusion mechanism of the inorganic ions onto the activated carbon surface *via* a pore-filling mechanism,[44] gave decreasing values of the saturation capacity as the adsorbent dosage increases from 25 mg to 100 mg.

Thus, of all the four isotherm models used in fitting the data, the Freudlich isotherms gave the best fits to the experimental data obtained for the adsorption modelling compared to the other three models and can therefore be used to describe the mechanism of the adsorption process as a multilayer adsorption process with surface heterogeneity[45] The obtained values of adsorption intensity n ranges between 0 and 1, thus indicating that the adsorption process is a chemisorption process. This is expected because the adsorption process cannot simply be explained as a reversible process involving metal ions occurring between solid and liquid phases.

Kinetic studies

The pseudo-first order and pseudo-second order reaction models expressed in Equations 9 and 10[46] were used for this study.[13]

$$\log\left(q_e - q_t\right) = \log q_e - \frac{k_{p1}}{2.303} t \quad (9)$$

$$\frac{t}{q_t} = \frac{1}{k_{p2} {q_e}^2} + \frac{1}{q_e} t \quad (10)$$

where q_e and q_t are the adsorption capacities (mg/g) at equilibrium and any time t respectively, k_{p1} (min^{-1}) and k_{p2} (g/(mg.min)) are the rate constants for both pseudo-first order and pseudo-second order reactions, respectively.

The graphs at different adsorbent dosage are shown in Figures 9(a)–(d) for the pseudo-first order for PET-H_2SO4. Figures 10(a)–(d) show the plots for the pseudo-second order model. The kinetic rate constants and error functions are highlighted in Table 4.

A comparison of the coefficient of determination values (R^2) for both reaction models shows that the pseudo-second order equation perfectly fits the adsorption data with R^2 values greater than 0.99 for all cases of varying adsorbent dosage and adsorbate concentrations. Hence, it is reasonable to conclude that the adsoprtion of manganese ions onto the activated carbon surface AC follows a second order kinetics whose rate law is expressed by Equation 10 and the adsorption process highlighted in Equation 11:

$$2AC + (MnO_4)^- + 5e^- \leftrightarrow MnAC_2 + 4O^- \quad (11)$$

where AC is the active sites on the carbon surface.

The chemical adsorption process occurs *via* the exchange of electrons between the carbon and manganese ions, whereby the driving force $(q_e - q_t)$ is proportional to the fraction of available active sites.[47–49] The change in oxidation state is

Table 4. Kinetic rate parameters for pseudo-first and pseudo-second order reaction models for PET-H_2SO_4 at 450 °C, 60 mins, 1.25 M.

Adsorbent dosage (mg)	Pseudo-first order constants											
	25 mg/L			50 mg/L			75 mg/L			100 mg/L		
	k_{p1} (min^{-1})	q_e (mg/g)	R^2	k_{p1} (min^{-1})	q_e (mg/g)	R^2	k_{p1} (min^{-1})	q_e (mg/g)	R^2	k_{p1} (min^{-1})	q_e (mg/g)	R^2
25	0.071	36.60	0.935	0.060	39.53	0.716	0.052	88.19	0.841	0.058	113.41	0.900
50	0.050	5.51	0.949	0.057	9.03	0.940	0.057	12.08	0.892	0.069	12.08	0.913
75	0.074	3.31	0.989	0.042	2.73	0.932	0.036	3.12	0.862	0.032	2.91	0.825
100	0.053	0.35	0.970	0.061	0.70	0.995	0.065	1.83	0.878	0.057	1.75	0.877

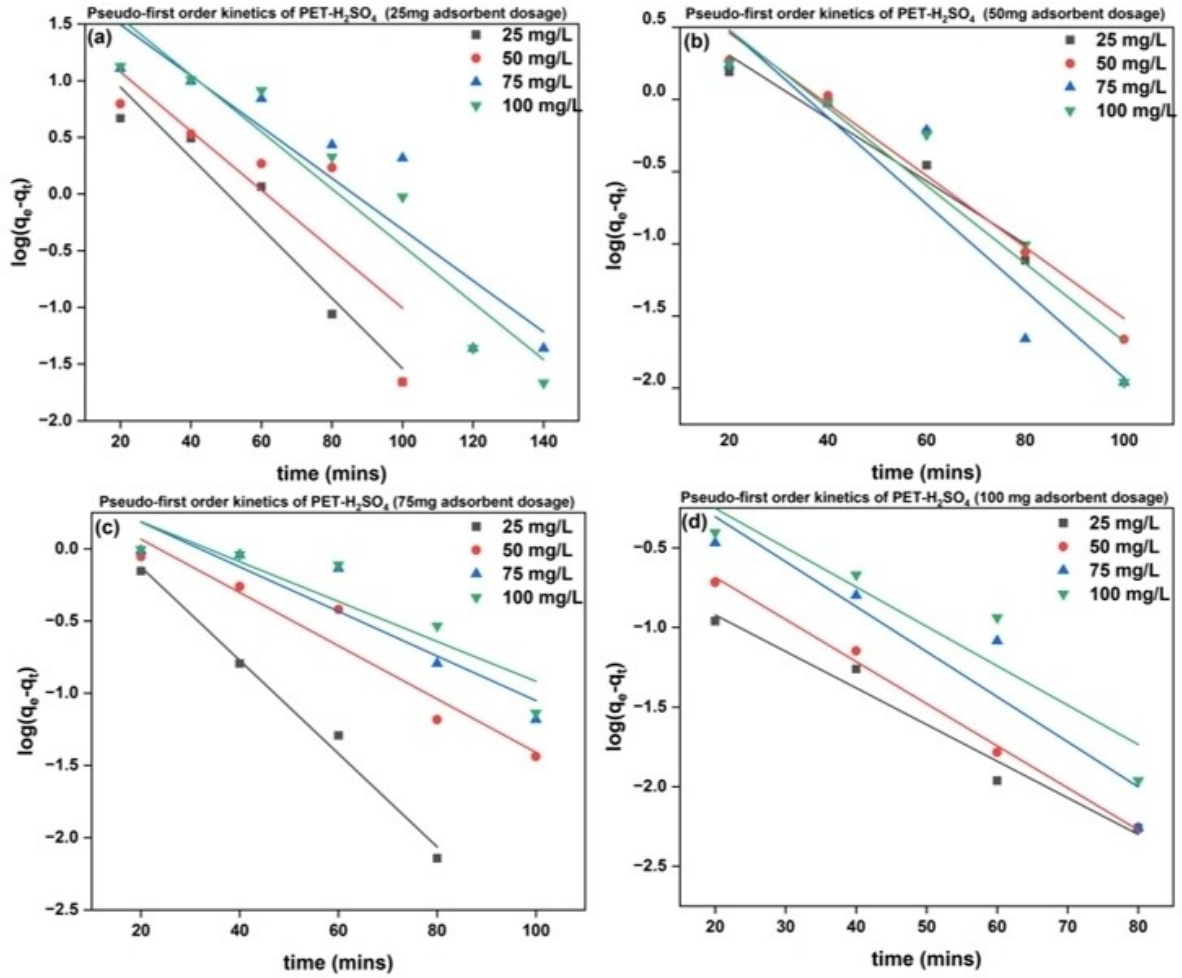

Figure 9. Pseudo-first order rate graphs for PET-H_2SO_4 at different adsorbent dosage (a) 25 mg (B) 50 mg (C) 75 mg (D) 100 mg (solid lines are fittings to the model).

evident in the UV-Vis analysis at an absorption band of 525.5 nm as there was no absorption at this wavelength at time $t=0$. The reduction of these ions occur *via* the formation of complexes with the oxygen functional groups on the carbon surface. In particular, the oxygen functional groups present on the carbon surface are involved in the chemical bonding, which influences the cationic exchange capacity of the carbon. In this case, the oxyl-groups donate electron pairs to manganese ions, forming coordination complexes.

From the data in Table 4, it is possible to observe that there is an increase in the reaction rate constant k_{p2} from 0.006 g/(mg.min) to 0.331 g/(mg.min) as the adsorbent dosage increases from 25 mg to 100 mg at an adsorbate concentration of 25 mg/L, thus, suggesting that higher adsorbent dosage has faster kinetic adsorption of manganese ions. This is the same for all cases of adsorbate concentration (50 mg/L, 75 mg/L, and 100 mg/L).

Diffusion studies

Diffusion in liquids[50,51] plays a key role in determining transport properties and can affect the overall kinetics of a process. In order to determine if the kinetic process is controlled by either film diffusion or intraparticle diffusion, two diffusion models, the Webber-Morris[46,52,53] and Dumwald-Wagner models,[54] were studied, which are shown in Equations (12) and (13), respectively.

$$q_t = k_{int} t^{1/2} \tag{12}$$

where k_{int} is the Webber-Morris intraparticle diffusion constant, and:

$$log\left(1 - \left(\frac{q_t}{q_e}\right)^2\right) = -\frac{K}{2.303} t \tag{13}$$

where K is the Dumwald-Wagner rate constant.

The rate-limiting step of the adsorption process is determined by the linearity or otherwise of the diffusion plots shown

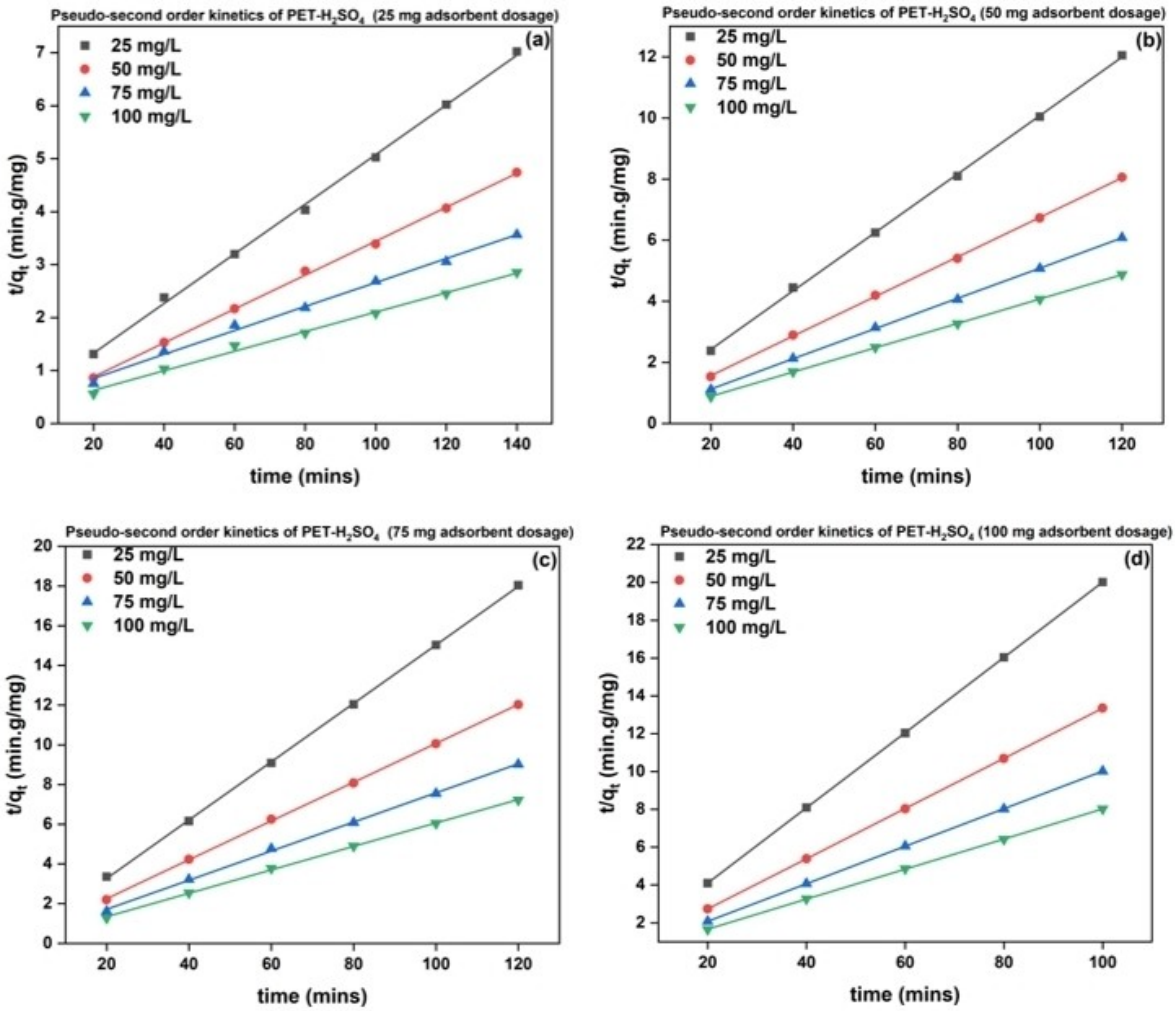

Figure 10. Pseudo-second order rate graphs for PET-H_2SO_4 at different adsorbent dosage (a) 25 mg (b) 50 mg (c) 75 mg (d) 100 mg (solid lines are fittings to the model).

in Figures 11 and 12, and also by their intercept values. The plots of q_t against $t^{1/2}$ and $\log\left(1-\left(\frac{q_t}{q_e}\right)^2\right)$ against t must pass through their origins if the sole rate limiting step were to be by intraparticle diffusion only.[46] However, this is not the case here as the plots showed different intercept values, thus implying that the adsorption kinetics of manganese ions on activated carbon surface is controlled by a multi-kinetic stage adsorption process.[38] The calculated rate parameters for both diffusion models are shown in Table 5.

Conclusions

The developing interest in plastics waste recycling has led to production of different fuels and carbon products. The

Table 5. Diffusion rate parameters for PET-H_2SO_4 at 450 °C, 60 mins, 1.25 M.

Adsorbent dosage (g)	Webber-Morris intraparticle diffusion constants							
	25 mg/L		50 mg/L		75 mg/L		100 mg/L	
	k_{int} mg/(g.(min$^{1/2}$))	R^2	k_{int} mg/(g.(min$^{1/2}$))	R^2	k_{int} mg/(g.(min$^{1/2}$))	R^2	k_{int} mg/(g.(min$^{1/2}$))	R^2
0.25	0.578	0.817	0.749	0.880	1.721	0.945	1.831	0.911
0.50	0.254	0.917	0.299	0.935	0.278	0.922	0.280	0.933
0.75	0.097	0.724	0.143	0.954	0.175	0.894	0.174	0.909
1.00	0.020	0.908	0.034	0.865	0.063	0.943	0.074	0.968

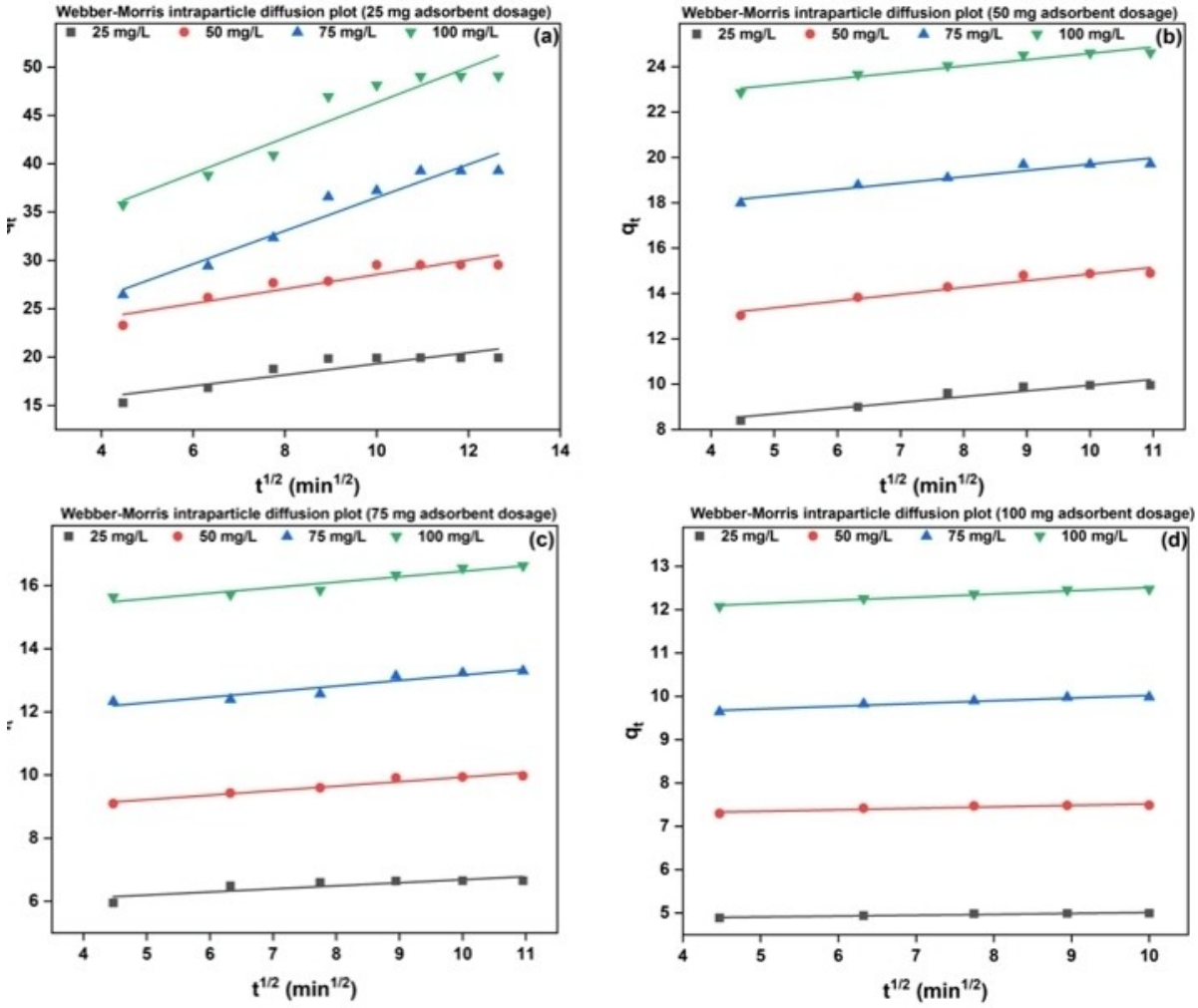

Figure 11. Webber-Morris kinetic graphs for PET-H_2SO_4 at different adsorbent dosage (a) 25 mg (b) 50 mg (c) 75 mg (d) 100 mg (solid lines are fittings to the model).

production of activated carbon from post-consumer polyethylene (PET) bottles is a waste management strategy for the removal of polymeric wastes from the environment, and also serves as a viable alternative for the manufacture of commercial activated carbons in water treatment processes.

The even dispersion of chemical activating agents onto the carbon surface leads to an even distribution of pore structures and also increases their adsorption capacities towards manganese, chromium, and cobalt ions.

Freundlich adsorption isotherms, pseudo-second order reaction model and the Webber-Morris intraparticle diffusion models were used to describe the adsorption of manganese ions onto the chemical activated carbons, whose rate-limiting steps are controlled by a multi-kinetic stage adsorption process involving both film and intraparticle diffusion.

The chemical waste recycling studies reported here will provide an alternative to the use of expensive commercial activated carbon, enhance circular economy, and proffers a viable way of removing the ubiquitous PET bottles from the environment. Future directions in this area will be focused on investigating the possibility to reuse the spent carbon materials in order to further minimize waste and enhance sustainability.

Experimental procedure

Materials

Potassium hydroxide (KOH) and sulphuric acid (H_2SO_4) were purchased from Sigma-Aldrich. Potassium iodide (KI), hydrochloric acid (HCl), starch soluble, iodine crystals, sodium thiosulphate ($Na_2S_2O_3{\cdot}5H_2O$), potassium permanganate ($KMnO_4$), cobalt (II) chloride ($CoCl_2$), and potassium dichromate (VI) ($K_2Cr_2O_7$) were of analytical grade. Post-consumer PET bottles are household waste drink bottles of different types and sizes. They were rinsed with water, dried at room temperature, fused at 100 °C, cooled and mechanically crushed into pieces and sieved using a mesh of 4 mm.

Pyrolysis and chemical activation

The crushed PET wastes were subsequently loaded into a pyrolysis flow reactor attached to a condensing unit. The pyrolysis temper-

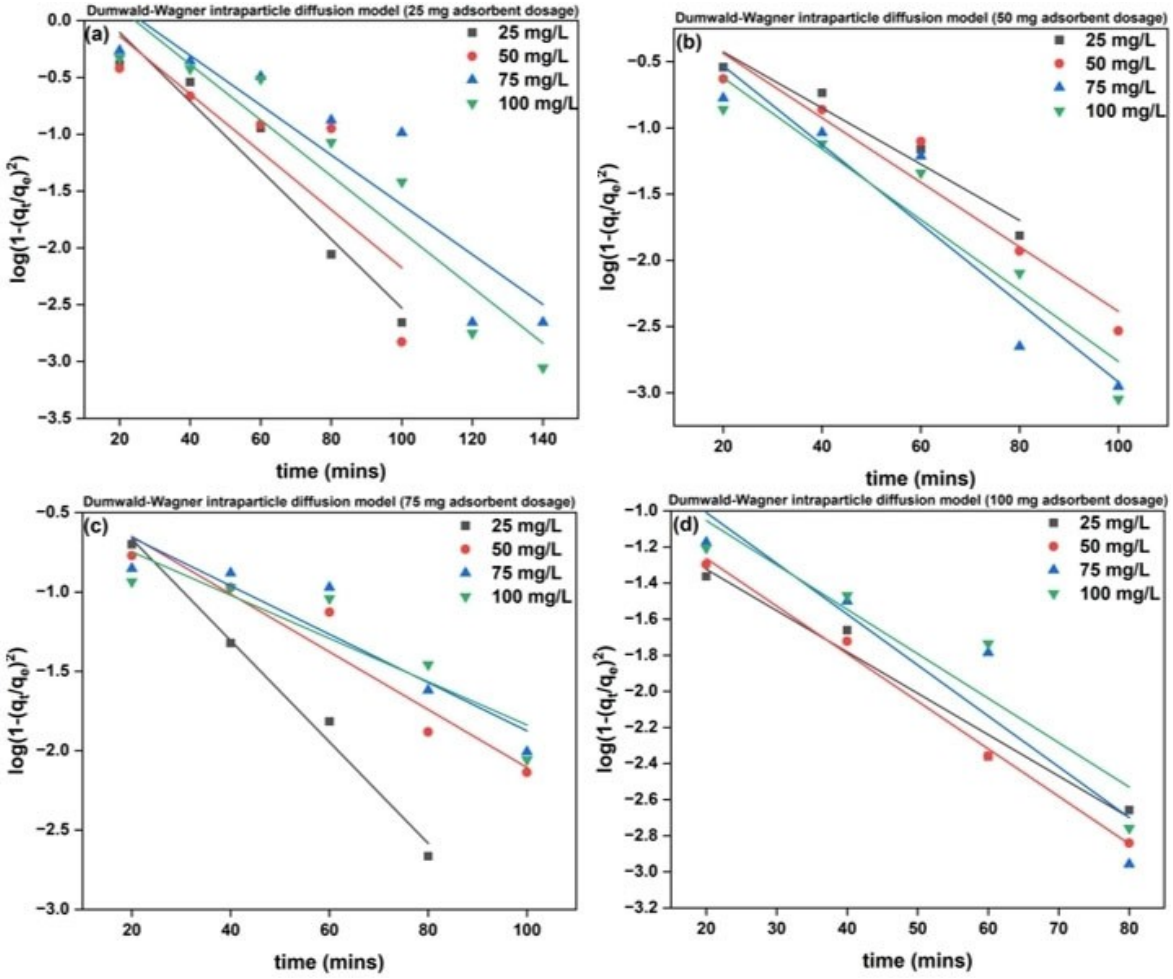

Figure 12. Dumwald-Wagner kinetic graphs for PET-H_2SO_4 at different adsorbent dosage (a) 25 mg (b) 50 mg (c) 75 mg (d) 100 mg (solid lines are fittings to the model).

ature was varied between 400 °C, 450 °C, and 500 °C, and the pyrolysis time was varied between 45–60 mins. The carbon produced was further activated and the effects of chemical activation was studied by the use of both acid (H_2SO_4) and base (KOH) activating agents at different concentrations 0.5 M, 1.25 M, and 2.0 M. Chemical activation was done in a Carbolite muffle furnace at 550 °C for a period of 30 mins, after which the activated carbons were rinsed repeatedly with deionized water to remove excess activating agents and residual inorganic impurities. Subsequently, they were dried and stored in a closed container for characterization and adsorption experiments. Tables 1 and 2 shows the experimental parameters for both H_2SO_4 and KOH activation, respectively.

Activated carbon characterization

The physico-chemical properties, such as, yield, moisture content (ASTM D2867-09), ash content (ASTM D2866-94), bulk density,[24] and iodine value (ASTM D4607-14) of the different activated carbons were obtained using standard ASTM procedure. Fourier Transform Infrared (FTIR) analysis was performed using Bruker Vertex 70 FTIR system. The crystallinity of the catalysts was determined using X-ray diffraction (PANanlytical XRD5). The surface area of the activated carbons were obtained using BET analysis of nitrogen sorption isotherms (Micrometrics ASAP 2020 static low pressure volumetric adsorption unit). Thermogravimetric analysis (TGA) of PET wastes was carried out under an inert atmosphere of nitrogen gas at heating rates of 5, 10 and 20 °C/min in order to obtain the decomposition profile of the waste polymer using a TGA Q5000 (TA Instrument).

Adsorption and kinetic studies

Batch adsorption studies were used to evaluate the adsorption performance of the activated carbons. Twenty-five (25) ppm solution of potassium per manganate ($KMnO_4$), potassium dichromate (VI) ($K_2Cr_2O_7$) and cobalt (II) chloride ($CoCl_2$) were prepared separately in a 250 mL volumetric flask using deionized water. A standard calibration curve was prepared for each ion. About 25 mg of adsorbent (chemically activated carbon) was weighed into 100 mL of the simulated water mixture and was put onto a rotary shaker with a speed of 150 rpm for 120 mins. The pH was adjusted to between 6.5 and 7. At the end of the reaction time, the solution was filtered using 0.2 μm PTFE. The absorbance of the filtrate was obtained with a UV-Visible spectrophotometer and the respective concentrations were obtained using Beer-Lambert Law. The wavelengths of absorption for Mn^{2+}, $Cr^{3+}$and Co^{2+} are 525.5 nm, 431 nm, and 351 nm, respectively. The percentage removal of each ion from water are obtained from Equation 14:

$$\%\ removal = \frac{C_0 - C_f}{C_0} \times 100 \quad (14)$$

where C_0 and C_f are the initial and final concentrations of the adsorbate in solution, respectively.

Afterwards, the activated carbon with the best adsorption capacity was used for further adsorption isotherm and kinetic studies in the removal of manganese ions from simulated water solutions. The isotherm studies were carried out by taking out 2 mL aliquots of the samples taken at 20 mins interval from a freshly prepared 25 ppm solution. The aliquots were filtered and the corresponding absorbance was obtained. The procedure was repeated for 50, 75, and 100 ppm solutions while also varying the adsorbent dosage at 50 mg, 75 mg, and 100 mg of carbon. The adsorption capacity was evaluated using Equation 15:

$$Adsoprtion\ capacity\ q_t = \frac{C_0 - C_t}{M} \times V \quad (15)$$

where C_0 is the initial concentration of the adsorbate (mg/L), C_t is the concentration at time t, M is the mass of the adsorbent, and V is the volume of the aqueous solution. Adsorption isotherm models were obtained using Langmuir, Freudlich, Temkim, and Dubnin-Radushkevich models.[55–57] Kinetic studies were carried out after an equilibrium of 140 hours using the pseudo-first order, pseudo-second order, and intraparticle diffusion models[46,58,59]

Acknowledgements

Olajumoke Alabi-Babalola would like to thank the Petroleum Technology Development Fund (PTDF), Nigeria for fully funding her PhD programme at The University of Manchester.

Conflict of Interests

The authors declare that there are no competing interests associated with this paper.

Data Availability Statement

The data that support the findings of this study are available from the corresponding author upon reasonable request.

Keywords: Activated carbon · Adsorption · Chemical plastic recycling · PET waste bottles · Pyrolysis

[1] A. A, Garforth, S. Ali, J. Hernandez-Martinez, A. Akah, *Curr. Opin. Solid State Mater. Sci.* **2004**, *8*, 419–425.
[2] G. Burillo, R. L. Clough, T. Czvikovszky, O. Guven, A. Le Moel, W. Liu, A. Singh, J. Yang, t. Zaharescu, *Radiat. Phys. Chem.* **2002**, *64*, 41–51.
[3] D. Mangaraj, *Rubber Chem. Technol.* **2005**, *78*, 536–547.
[4] P. Subramanian, *Resour. Conserv. Recycl.* **2000**, *28*, 253–263.
[5] A. bin Jumah, A. A. Tedstone, A. A. Garforth, *Microporous Mesoporous Mater.* **2021**, *315*, 110912.
[6] O. Alabi-Babalola, E. F. Aransiola, T. Shittu, *Adv. Chem. Eng. Sci.* **2021**, *11*, 38.
[7] K. Lan, Y. Yao, *Comm. Earth & Envronment.* **2022**, *3*, 300.
[8] S. Chari, A. Sebastiani, A. Paulillo, M. Materazzi, *ACS Sustainable Chem. Eng.* **2023**, *11*, 3248–3259.
[9] J. Y. Teo, A. Ong, T. T. Y. Tan, X. Li, X. J. Loh, J. Y. C. Lim, *Green Chem.* **2022**, *24*, 6086–6099.
[10] F. Hussin, M. K. Aroua, M. A. Kassim, U. F. Md. Ali, *Energies.* **2021**, *14*, 8421.
[11] L. P. Mata Costa, L. D. M. Vaz de Miranda, A. C. Couto de Oliveira, L. Falcon, M. S. S. Pimenta, I. G. Bessa, S. J. Wouters, M. H. S. Andrade, J. C. Pinto, *Processes* **2021**, *9*, 759.
[12] J. Idris, G. D. Eyu, Z. Ahmad, C. S. Chukwuekezie, *Aust. J. Basic Appl. Sci.* **2013**, *7*, 272–280.
[13] J. Saleem, M. A. Riaz, M. Gordon, *J. Hazard. Mater.* **2018**, *341*, 424–437.
[14] J. Saleem, Z. K. B. Moghal, R. A. Shakoor, G. McKay, *Int. J. Mol. Sci.* **2023**, *24*, 12368.
[15] J. Saleem, C. Ning, J. Bradford, G. McKAy, *Waste Manage.* **2015**, *44*, 34–38.
[16] C. Yu, W. Lin, J. Jiang, Z. Jing, P. Hong, Y. Li, *RSC Adv.* **2019**, *9*, 37759–37767.
[17] A. K. Aboul-Gheit, F. H. Khalil, T. Abdel-Moghny, *Oil Gas Sci. Technol.* **2006**, *61*, 259–268.
[18] J. B. Williamson, S. E. Lewis, R. R. Johnson III, I. M. Manning, F. A. Leibfarth, *Angew. Chem. Int. Ed. Engl.* **2019**, *58*, 8654–8668.
[19] C. Yeung, W. W. Loh, H. H. Lau, X. J. Loh, *Mater. Today Chem.* **2021**, *21*, 100524.
[20] X. Dong, A. Akram, B. Comesana-Gandara, *ACS Appl. Polym. Mater.* **2020**, *2*, 2586–2593.
[21] S. Chaudhary, M. Kumari, P. Chauhan, G. R. Chaudhary, *Waste Manage.* **2021**, *120*, 675–686.
[22] J. Y. Q. Teo, X. T. Zheng, D. H. L. Seng, H. K. Hui, P. L. Chee, X. Su, X. J. Loh, J. Y. C. Lim, *ChemistrySelect* **2022**. *7*, e202202720.
[23] S. Shin, J. Jang, S. H. Yoon, I. Mochida, *Carbon.* **1997**, *35*, 1739–1743.
[24] Z. Al-Qodah, R. Shawabkah, *Braz. J. Chem. Eng.* **2009**, *26*, 127–136.
[25] F. Ademiluyi, S. Amadi, N. J. Amakama, *J. Appl. Sci. Environ. Manage.* **2009**, *13*.
[26] A. Buasri, N. Chaiyut, V. Loryuenyong, E. Phakdeepataraphan, S. Watpathomsub, *Int. J. Mater. Metall. Eng.* **2013**, *7*, 106–110.
[27] Y. Wang, H. Wang, S. Li, S. Sun, *ACS Omega* **2022**, *7*, 35180–35190.
[28] X. Yuan, M. K. Cho, J. G. lee, S. W. Choi, K. B. Lee, *Environ. Pollut.* **2020**, *265*, 114868.
[29] M. Y. Tan, L. Goh, D. Safanama, W. W. loh, N. Ding, S. W. Chien, S. S. Goh, W. Thitsartam, J. Y. C. Lim, *J. Mater. Chem. A.* **2022**, *10*, 24468–24474.
[30] X. Cheng, J. Pan, Y. Zhao, M. Liao, H. Peng, *Adv. Energy Mater.* **2018**, *8*, 1702184.
[31] N. Goujon, J. Demarteau, X. Lopez de Pariza, N. Casado, H. Sardon, D. Mecerreyes, *Sustainable Chem.* **2021**, *2*, 610–621.
[32] K. Chan, A. Zinchenko, *J. Environ. Chem. Eng.* **2022**, *10*, 108055.
[33] K. Chan, A. Zinchenko, *J. Environ. Chem. Eng.* **2021**, *9*, 106129.
[34] S. Venkatachalam, S. G. NAyak, J. V. Labde, P. R. Gharal, K. Rao, A. K. Kelkar, *books.google.com.* **2012**, InTech Rijeka, Croatia.
[35] C. Saka, *J. Anal. Appl. Pyrolysis.* **2012**, *95*, 21–24.
[36] A. Üçer, A. Uyanik, Ş. Aygün, *Sep. Purif. Technol.* **2006**, *47*, 113–118.
[37] A. Omri, M. Benzina, *Alexandria Eng. J.* **2012**, *51*, 343–350.
[38] T. N. Tran, D. G. Kim, S. O. Ko, *KSCE J. Civ. Eng.* **2018**, *22*, 3772–3782.
[39] M. Arshadi, M. J. Amiri, S. Mousavi, *Water Resour. Ind.* **2014**, *6*, 1–17.
[40] J. M. O'reilly, R. A. Mosher, *Carbon* **1983**, *21*, 47–51.
[41] V. Ţucureanu, A. Matei, A. M. Avram, *Crit. Rev. Anal. Chem.* **2016**, *46*, 502–520.
[42] T. W. Weber, R. K. Chakravorti, *AIChE J.* **1974**, *20*, 228–238.
[43] F. Haghseresht, G. Lu, *Energy Fuels.* **1998**, *12*, 1100–1107.
[44] K. Y. Foo, B. H. Hameed, *Chem. Eng. J.* **2010**, *156*, 2–10.
[45] A. Adamson, J. Klerer, *J. Electrochem. Soc.* **1977**, *124*, 192C.
[46] H. Qiu, L. Lv, B. Pan, Q. Zhang, Q. Zhang, *J. Zhejiang University-Science A* **2009**. *10*: p. 716–724.
[47] Y. S. Ho, *J. Hazard. Mater.* **2006**, *136*, 681–689.
[48] T. D. Shittu, E. F. Aransiola, O. D. Alabi-Babalola, *J. Environ. Prot.* **2020**, *11*, 65.
[49] Y. S. Ho, *Water Res.* **2006**, *40 (1)*, 119–125.
[50] Q. Zhu, G. D. Moggridge, C. D'Agostino, *Chem. Eng. Sci.* **2015**, *132*, 250–258.
[51] C. D'Agostino, J. A. Stephens, J. D. Parkinson, *Chem. Eng. Sci.* **2013**, *95*, 43–47.
[52] W. J. Weber Jr, J. C. Morris, *J. Sanit. Eng. Div.* **1963**, *89*, 31–59.

[53] M. Alkan, M. Dogan, Y. Turhan, O. Demirbas, P. Turan, *Chem. Eng. J.* **2008**, *139*, 213–223.
[54] H. L. Wang, J. L. Chen, Z. C. Zhai, *Environ. Chem. Beijing.* **2004**. *23*, 192–196.
[55] N. Ayawei, A. N. Ebelegi, D. Wankasi, *J. Chem.* **2017**. *201*, 3039817.
[56] O. D. Alabi-Babalola, E. F. Aransiola, T. D. Shittu, *Ife J of Tech.* **2019**. *26*, 34–46.
[57] T. D. Shittu, E. F. Aransiola, O. D. Alabi-Babalola, *J Bioremediat Biodegrad* **2020**. *11*, 2.
[58] Q. Zhu, G. D. Moggridge, C. D'Agostino, *Chem. Eng. J.* **2016**, *306*, 67–76.
[59] Q. Zhu, G. D. Moggridge, C. D'Agostino, *Part 2: Kinetics and diffusion analysis. Chem. Eng. J.* **2016**. *306*, 1223–1233.

Manuscript received: August 30, 2023
Revised manuscript received: November 30, 2023
Version of record online: ■■, ■■

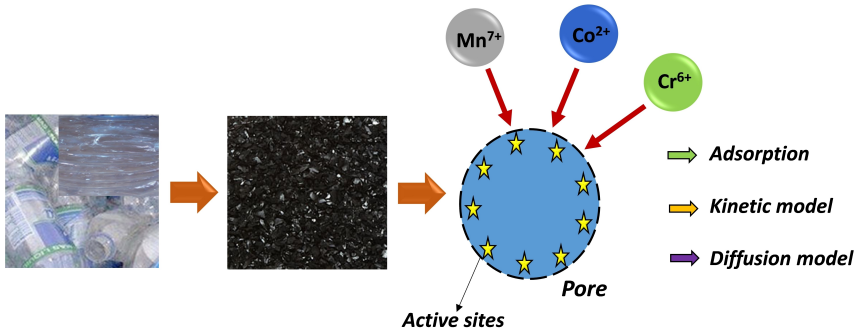

*O. Alabi-Babalola, Dr. E. Aransiola, Dr. E. Asuquo, Dr. A. Garforth, Dr. C. D'Agostino**

1 – 15

Production of Highly Efficient Activated Carbons for Wastewater Treatment from Post-Consumer PET Plastic Bottle Waste

Special Collection

Our work involves the conversion of PET waste bottles into activated carbons through pyrolysis, followed by chemical modifications of the carbon surface functionality with oxygen-containing groups. The produced carbons are then used for removal of inorganic ions from wastewater. The results show that activated carbons from PET waste bottles are a sustainable waste management control strategy for eliminating non-biodegradable wastes from the environment.